JOURNAL OF SOLID STATE CHEMISTRY **125,** 171–177 (1996)
ARTICLE NO. 0281

Equation of State of Potassium Hydrogen Fluoride to 12.3 GPa and Stability of *I*4/*mcm* Structure to 50 GPa: An Energy-Dispersive X-Ray Diffraction Study

Andrew G. Christy*,† and Simon M. Clark†

*Research School of Chemistry, The Australian National University, Canberra, ACT 0200, Australia; and †Daresbury Laboratory, Daresbury, Warrington WA4 4AD, England

Received February 19, 1996; accepted May 16, 1996

Potassium hydrogen fluoride (KHF_2) crystallizes in the tetragonal system, space group *I*4/*mcm*, $Z = 4$, $a = 5.668(2)$ Å, $c = 6.801(7)$ Å, under ambient conditions. Energy-dispersive X-ray diffraction was used to study the compression behavior of KHF_2 in a diamond anvil cell. Unit cell parameters were determined at ten different static pressures between 1 atm and 12.3 GPa, and the calculated cell volumes were found to fit a third-order Birch–Murnaghan equation of state with $K_0 = 25.1(15)$ GPa and $K' = 10.0(19)$. The compressibility is greatest by a factor of two parallel to z despite the short K–K distances in this direction, implying that F–F repulsion controls the compressibility behavior. A reconnaissance study to much higher pressure showed that KHF_2 remains in this structure down to 67.6% of its ambient volume, at a pressure estimated as 50 GPa. The tetragonal structure appears to be stable at higher P than the *a*3 pyrite structure, which is unlikely to have a stability field for KHF_2. The high-pressure stability of the *I*4/*mcm* structure is not surprising given that it is effectively the same as that of the highly coordinated $CuAl_2/Fe_2B$ group of intermetallics. In contrast, AX_2 compounds without X–X bonding adopt Ni_2In-like structures at high pressure. Electron density studies and modeling suggest that the distinction between these two groups of compounds may not be rigid.

INTRODUCTION

Potassium hydrogen fluoride (KHF_2) contains symmetrical, strongly hydrogen-bonded $[FHF]^-$ ions with a very short F–F distance of 2.26 Å (1). The crystal structure of KHF_2 (Fig. 1) is tetragonal with space group *I*4/*mcm* under ambient conditions (2) but becomes cubic on heating to 196.7°C. The time-averaged structure of the high-temperature phase is the B1 (rocksalt) structure, achieved by the disordering of [FHF] group orientations between each of the four ⟨111⟩ directions. Therefore, there is a local resemblance to the *Pa*3 structure of pyrite, in which linear anions are statically ordered along these directions. The transformation is accompanied by a large increase in electrical conductivity; the low-temperature phase is a protonic conductor, whereas K+, F-, and [FHF]- groups are all very mobile in the cubic phase (3–5). A high-pressure conductivity study by Bradley *et al.* (6) traced the tetragonal–cubic transition up to 5.7 GPa, where it occurred at 245°C. The near-isothermal slope in P–T space for this transition is a consequence of the large entropy increase on formation of the cubic phase (23.8 J/mol K; 7, 8) despite the large volume increase (+12.7% at 1 bar). There is a possibility of ordered pyrite-like KHF_2 being stable at high pressure and lower temperatures than the disordered structure or the tetragonal phase. Orientational ordering causes a 13% volume decrease in NaSH (9). Such a volume change combined with loss of configurational entropy might be sufficient to change the slope of the tetragonal–cubic equilibrium curve in P–T space. Even a change from dynamic to static orientational disorder causes a large change in the slope of an equilibrium line in $CsCuCl_3$ (10). However, taking the F–H–F distance to be 2.26 Å and assuming the K–F distance for sixfold coordinated K to be the same as in KF (2.66 Å), the cell parameter for a hypothetical *Pa*3 KHF_2 at ambient is estimated to be 6.30 Å, very close to that of the dynamically disordered cubic phase and substantially larger than that of the tetragonal phase. The lack of contraction on ordering may be a consequence of the four [FHF] orientations spanning all three dimensions rather than just a single plane or axis.

The much smaller volume of the tetragonal structure renders it increasingly stable relative to pyrite with increasing pressure, as is consistent with the derivation of the two structures from the B2 (CsCl) and B1 (rocksalt) structures, respectively, by substitution of [FHF] groups for monoatomic anions. The nearly isothermal equilibrium between ordered and disordered pyrite structures, and the known stable equilibrium between the disordered phase and the tetragonal phase at 1 atm, together imply that the ordered pyrite phase does not have a stability field at positive pressure for KHF_2.

0022-4596/96 $18.00

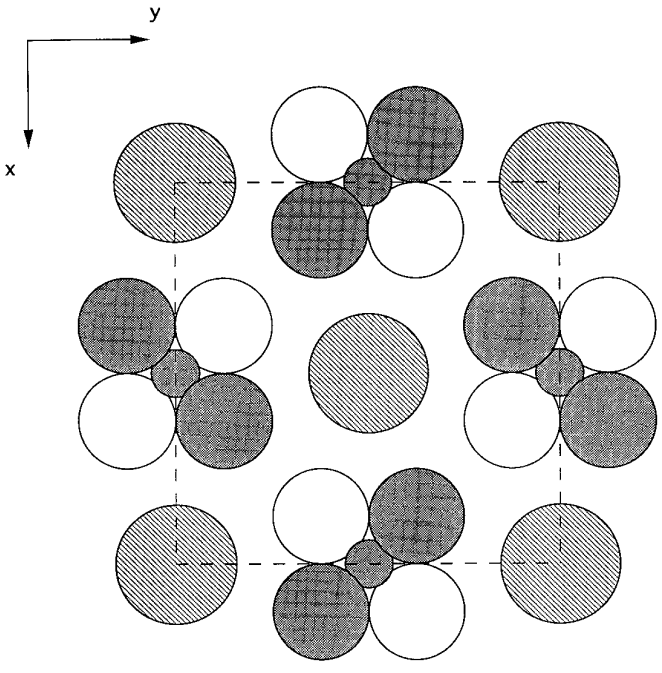

FIG. 1. The tetragonal structure of KHF_2 projected onto (001). K atoms (large circles, shaded) at $z = \pm\frac{1}{4}$, F (medium) and H (small) at $z = 0$ (white) and $z = \frac{1}{2}$ (stippled).

The compound $NaHF_2$ also adopts the disordered pyrite structure at high temperature, but occurs as a rhombohedral variant at ambient, with all anions aligned along a unique triad axis. In an earlier study (11) it was shown that this compound undergoes two transitions below 4 GPa, and the structures of the high-pressure phases were identified as marcasite-like (0.4–4.0 GPa) and similar to tetragonal KHF_2 (>4 GPa). Observation of the latter phase is not surprising since high-pressure phases are often similar in structure to the low-pressure phases of compounds with similar stoichiometry but with larger and heavier atoms substituted (K for Na in this instance). A similar analogy may also be found between compounds of similar stoichiometry but differing formal ionic charge: The hydrogen fluorides show a strong similarity to disulfides in their structural behavior. If the bridging hydrogen atoms and minor structural distortions are neglected, the structure of $NaHF_2$-II resembles that of marcasite, the low-entropy, large-volume form of FeS_2 (12), $NaHF_2$-III and KHF_2 are isostructural with SrS_2 (13), and the high-temperature structure of $NaHF_2$ and KHF_2 is a dynamically disordered variant of that of pyrite (the high-entropy, small-volume form of FeS_2). Note that these structures may all be interconverted by simple sequences of atomic displacements, and are related to simple MO_2 oxide structures (rutile, fluorite) in which anion–anion bonds are absent (11, 14). It is reasonable to suppose that the structural behavior of KHF_2 may provide a model for that of both $NaHF_2$ and disulfides at much greater pressures, and hence may serve as a guide to what structures to expect in these compounds under extreme conditions.

EXPERIMENTAL

KHF_2 was obtained commercially (>99% pure) from Stren Chemicals, Inc. The sample was ground with a pestle and mortar together with NaCl which was used as an internal pressure calibrant. Two diamond anvil cells were used for high pressure generation: the first had 0.5 mm diameter anvil faces and was used to generate pressures up to 12.3 GPa; a second cell with 0.3 mm anvil faces was used to obtain higher pressures. Steel gaskets of initial thickness 200 μm were used to contain the samples, in holes of initial diameter 200 μm (lower pressure run) and 100 μm (higher pressure run). The calibrant and sample mixture was loaded into the cells with nujol as a quasihydrostatic pressure medium in order to avoid hydrolysis of the sample in the methanol–ethanol–water mixture normally used.

Powder X-ray diffraction spectra were collected at a series of static pressures using the energy-dispersive powder diffraction (EDPD) facility (15, 16) at the Daresbury Synchrotron Radiation Source (SRS). The SRS operates at 2 GeV with typical electron beam currents of about 200 mA. The EDPD facility was situated 15 m from the tangent point to the ring, with hard X-ray flux enhanced by a superconducting wiggler magnet with a 5 T peak field. The peak X-ray flux was at 10 keV, with about 7×10^{11} photons/s/mm^2 in a 0.1% bandwidth around that energy. The X-ray flux was high enough to be useful from about 5 to 70 keV. The EDPD method used a polychromatic beam of incident X-rays, and a solid-state Ge(Li) detector set at a fixed scattering angle 2θ, selected to be near 7° so as to maximize the known sample peaks in the useful energy range. 2θ was refined using a Si standard as 6.858° for the lower pressure data set of this study and 6.861° for the higher pressure data set. The fixed geometry allowed easy collection of data for a wide range of d spacings given the limited optical access to the sample in the diamond anvil cell. The high X-ray flux allowed short collection times per spectrum given the very small sample size: 1000 s per run in this case. The principal disadvantages of the EDPD method are that the energy resolution is an order of magnitude worse than obtainable using monochromatic techniques, and that features are recorded that do not arise from Bragg scattering within the sample. These include elemental fluorescences, Compton scattering from the diamonds, and escape peaks due to secondary scattering within the detector. EDPD is nevertheless well suited to fast reconnaissance of large pressure ranges.

Data were analyzed using the GENIE spectrum manipulation package (17). Parts of each spectrum were fitted by

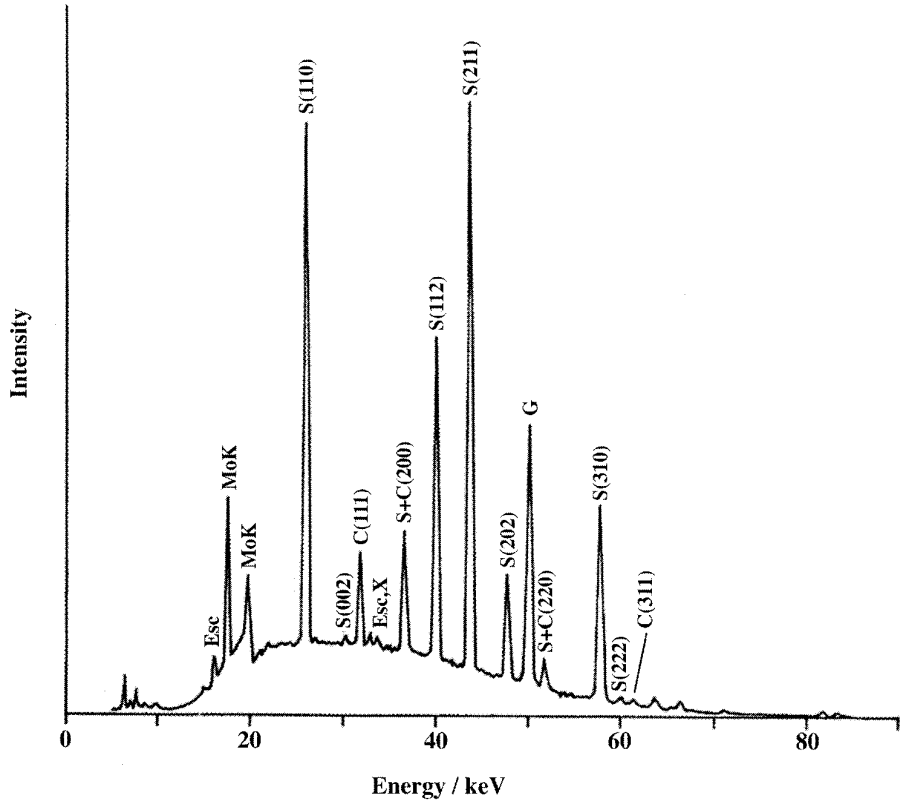

FIG. 2. The EDPD spectrum of KHF_2 collected under ambient conditions. Bragg peaks from sample are indicated by S(*hkl*), those from NaCl calibrant by C(*hkl*). Esc indicates escape peaks, Mo*K* indicates molybdenum fluorescence peaks, G indicates a gasket diffraction peak, and X indicates a diffraction peak from KF impurity.

up to five summed Gaussian curves superimposed on a parabolic background in order to accurately determine peak positions. Unit cell parameters were refined from fitted peak positions using the REFCEL program (18). Further analysis was carried out using the spreadsheet program EXCEL.

Sample pressure for the lower pressure (<20 GPa) data set was estimated using Decker's equation of state for sodium chloride (19). The 111 and 311 reflections were used, along with 200 and 220 which overlapped strongly with 200 and 220, respectively, of the sample, but were usually separable from the sample peaks using GENIE. The experimental error in pressure determination is estimated to be ±0.03 GPa at ambient, rising to ±0.1 GPa at about 10 GPa as the spectrum quality decreased.

RESULTS

Figure 2 shows an EDPD spectrum of a mixture of KHF_2 and NaCl contained in a diamond anvil cell at near-ambient pressure. In addition to diffraction peaks from the sample and calibrant, a gasket peak is visible (110 of the steel ferrite phase near 50 keV) as well as a weak peak from a KF impurity (33.6 keV). The strongest sample peaks (110 and 211) give rise to weak escape peaks about 10.3 keV lower in energy than the Bragg peaks. The K absorption edge (20 keV) and K_α (17.5 keV) and K_β (19.6 keV) fluorescences of molybdenum can be seen at 17–20 keV; these are produced in the post-sample collimator, which is made from 50-cm long Mo bars with a 0.1-mm gap between them.

Bragg peaks from the sample were indexed on the tetragonal cell for all spectra. Cell parameters up to 12.3 GPa were refined using the measured positions of the 110, 112, 211, 202, and 310 reflections, plus the 200 and 220 reflections once these were separated from the overlapping calibrant peaks. The unit cell parameters determined at ambient pressure, $a = 5.668(2)$ Å and $c = 6.801(7)$ Å, are in extremely good agreement with those of Carrell and Donohue (20). Cell parameter precision deteriorated with increasing pressure as the sample thinned, reducing peak heights relative to the background in the spectra. Unit cell parameters and volumes are presented in Table 1, and are shown graphically in Figs. 3 and 4.

The data for the runs up to 12.3 GPa pressure were fitted to a third-order Birch–Murnaghan equation of state (21, 22), with zero-pressure values as measured. The fitted values are presented in Table 2. The root mean square (r.m.s.) deviation between observed and calculated *P* val-

TABLE 1
Unit Cell Data for KHF_2

P/GPa	a/Å	c/Å	V_{cell}/Å^3
	Low-P data set		
0.0001	5.668(2)	6.801(7)	218.5(3)
0.62	5.629(6)	6.745(23)	213.7(8)
1.27	5.598(5)	6.682(21)	209.4(7)
1.63	5.586(2)	6.589(4)	206.9(3)
2.23	5.566(1)	6.516(8)	204.1(1)
3.22	5.538(2)	6.516(8)	199.8(3)
4.53	5.513(2)	6.453(9)	196.1(3)
5.65	5.486(3)	6.464(63)	194.5(19)
8.13	5.439(4)	6.277(84)	185.7(25)
12.3	5.346(23)	6.263(67)	179.0(22)
	High-P data set		
24.6(27)	5.127(16)	6.247(41)	164.2(13)
35.7(41)	5.051(13)	6.104(33)	155.7(10)
43.7(52)	4.995(2)	6.053(5)	151.0(2)
50.3(62)	4.960(2)	6.003(6)	147.7(2)

ues using the K_0 and K' values obtained was ±0.28 GPa. The large K' value is significant, since this fit was appreciably better than that using the second-order equation with K' constrained equal to 4. If V_0 is constrained as measured, the second-order equation gives K_0 = 37.6 GPa, with a r.m.s. deviation in P of ±0.62 GPa. If V_0 is refined, then k_0 = 43.6 GPa, V_0 = 215.2 Å^3 (1.5% smaller than measured), and the deviation in calculated P is still ±0.46 GPa.

Interpretation of the data from the higher pressure run presented some complications:

(i) The pressure increased very fast. The first spectrum obtained on increasing the pressure above ambient corresponded to a pressure of about 10 GPa, and was consistent with those obtained in the earlier data set. At higher pressures, the calibrant peaks were lost due to sample thinning or calibrant recrystallization.

(ii) Intense, broad (~1 keV FWHM) diffraction peaks appeared above 10 GPa at 47.7–48.3, 50.8–51.4, and 54.0–54.8 keV approximately, and an escape peak from the first of these at 37.4–38.0 keV. These obscured several sample and calibrant peaks. Nevertheless, the 110, 200, and 112 reflections from tetragonal KHF_2 remained visible up to the highest pressure attained.

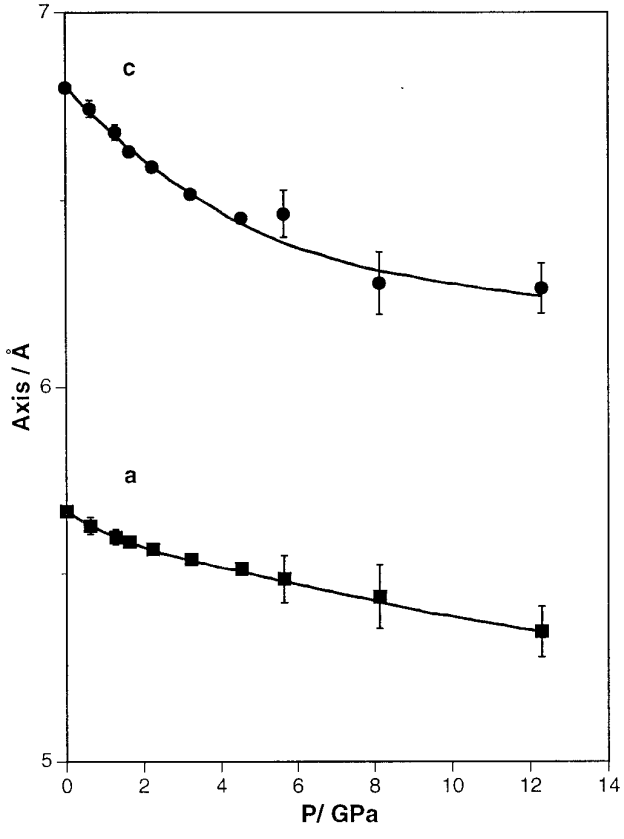

FIG. 3. Variation of KHF_2 cell parameters with pressure. The curve is a guide for the eye.

TABLE 2
Compressibility Data for KHF_2 at Atmospheric (Effectively, Zero) Pressure

Cell constants	a_0/Å	5.668(2)
	c_0/Å	6.801(7)
	V_0/Å^3	218.5(3)
Bulk modulus[a]	K_0/GPa	25.1(15)
Pressure derivative of K	K'	10.0(19)
Stiffness[b] $\parallel x$	/GPa	117(18)
Stiffness $\parallel z$	/GPa	51(9)

[a] K_0 and K' are those applicable for the equation $P = (\frac{3}{2})K_0u^5(u^2 - 1)\{1 + 3(K'/4 - 1)(u^2 - 1)\}$, where $u = (V_0/V)^{(1/3)}$.

[b] Axial stiffnesses derived using the Birch–Murnaghan equation of [a] but replacing u by (a_0/a) or (c_0/c) and replacing the constant $\frac{3}{2}$ with $\frac{1}{2}$. Pressure derivatives not quoted since estimated errors exceeded the magnitudes of the derivatives.

The new peaks appear to arise from the gasket, transformed into a hexagonal close-packed phase. Hexagonal close-packed ε-Fe is stable above 13 GPa at room temperature (23). Jephcoat *et al.* (24) give the cell parameters of ε-Fe at 13.27 GPa as a = 2.498 Å and c = 3.965 Å. Corresponding energies for the first three Bragg peaks in the higher pressure run of this study would be (100) 47.9 keV, (002) 52.3 keV, and (101) 54.6 keV. The observed peak energies are clearly comparable, particularly if their great width is taken into account, which is presumably due to inhomogeneous strain in the gasket.

The observed 002 reflection appears to be too low in energy relative to the other two peaks by about 1 keV, which is probably due to a combination of change in pre-

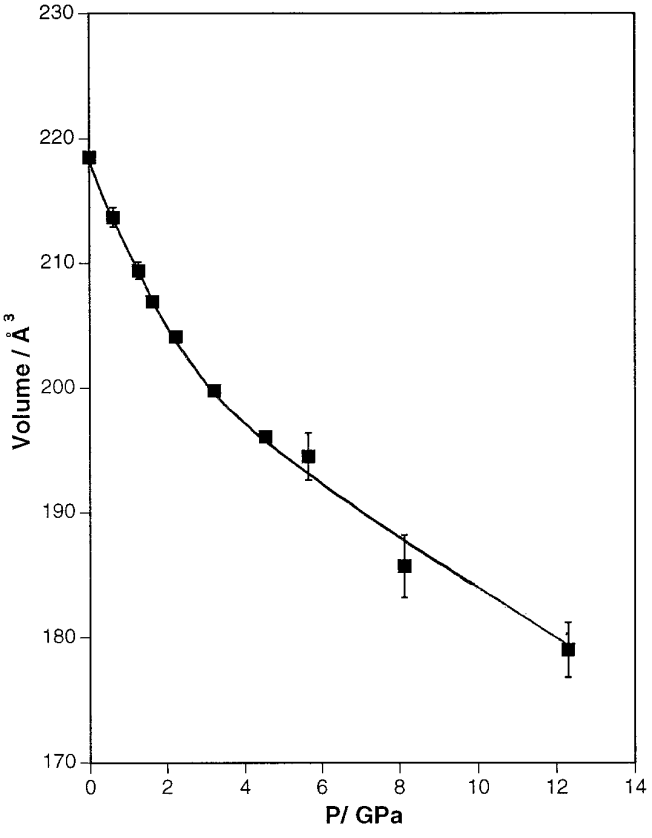

FIG. 4. Variation of KHF_2 unit cell volume with pressure.

ferred orientation of the gasket in different pressure regimes, nonhydrostatic stress, and overlap with the sample 211 peak.

Since no calibrant peaks were visible, the spectra were analyzed by plotting sample 200 and 112 peaks, and the new peaks, against the energy of the sample 110 reflection. The resulting plot may be seen in Fig. 5. The energy of the 200 sample peak is necessarily proportional to that of the 110 peak in these and the higher pressure runs. The observation that the 112 peak energies also vary smoothly with 110 energy implies that there are no discontinuities in the pressure evolution of the *cla* ratio, and hence no tetragonal–tetragonal phase transitions over the pressure range examined. Such isosymmetric transitions can occur at high pressure due to change in the dominant compression mechanism (25). The gasket peaks clearly change position much more slowly with increasing pressure than do the sample peaks.

Cell parameters were determined from the three visible sample peaks, and cell volumes were calculated from these. Values are given in Table 1 for comparison with the lower pressure data of the first run. It should be noted that the estimated errors quoted are artificially low due to the small number of peak positions used. Nevertheless, it is clear that much higher pressures were attained in the second run. At 12.3 GPa, the unit cell of KHF_2 has 81.9% of its volume at 1 bar, whereas the four high-pressure volumes of the second run range from 75.1 to 67.6% of atmospheric volume. Given the absence of calibrant peaks, quantitative estimates of sample pressure were made by extrapolating the sample equation of state previously determined over the interval 0–12.3 GPa. The sample pressures estimated by this method range from 24.6 to 50.3 GPa. Corresponding estimates assuming a more conservative second-order equation of state (K_0 = 37.6 GPa, K' = 4) are 19.4 and 32.9 GPa, respectively. We conclude that KHF_2 remains stable in the *I*4/*mcm* structure down to 67.6% of its volume at ambient. The corresponding sample pressure is higher than 30 GPa and is likely to be about 50 GPa.

DISCUSSION

The tetragonal structure of KHF_2 remains stable under extreme compression ($1 - V/V_0 \geq 0.327$, where V_0 is the

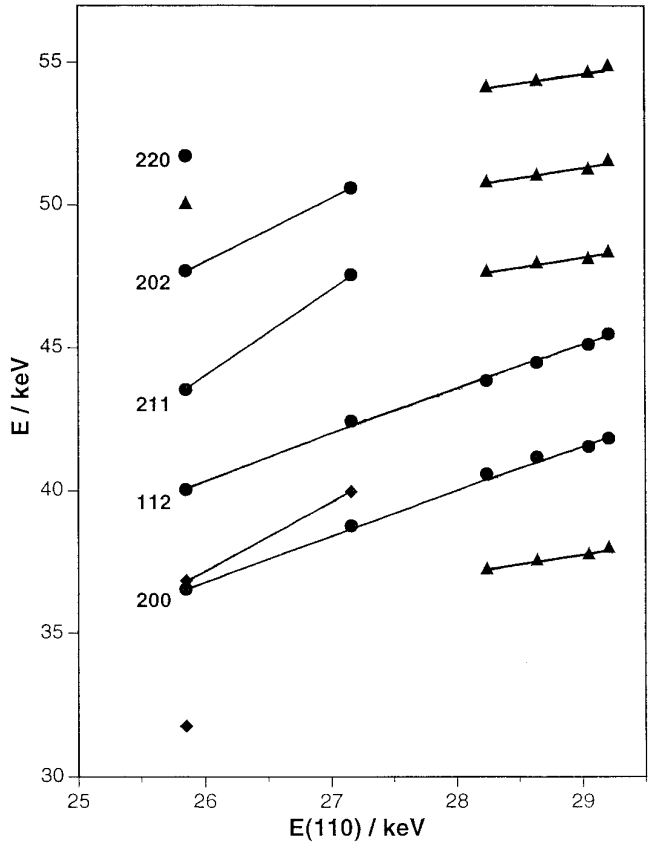

FIG. 5. The measured energies of peaks from the higher pressure data set plotted against the measured energy of the KHF_2 110 reflection. Sample peaks indicated by circles, calibrant peaks by diamond shapes, and gasket peaks by triangles.

volume at ambient). This contrasts with the behavior of $NaHF_2$, which undergoes two phase transitions below 4 GPa, eventually transforming into the tetragonal structure (11). KHF_2 is much more compressible than the near-isostructural polymorph of $NaHF_2$: the bulk modulus of $NaHF_2$-III at 4.16 GPa is 137 GPa (compare $K_0 = 25$ GPa for KHF_2). The difference is also reflected in the axial compressibilities. The linear [FHF] groups in $NaHF_2$-I and $NaHF_2$-II act as rigid braces down the **z** axis of the structure, a direction which is almost incompressible as a result.

The *xy* plane of KHF_2, in which the [FHF] lie in two orientations, is less compressible than the **z** direction but only by a factor of two over the pressure range 0–12.3 GPa (Table 2). A similarly small degree of anisotropy is seen in $NaHF_2$-III (11). The fact that the **z** direction is the most compressible in this structure contrasts with the observation that the cation–cation distances in the **z** direction are much shorter than those in the ⟨110⟩ directions (3.40 and 4.00 Å, respectively in KHF_2 under atmospheric pressure). This implies that the compressibility behavior is dominated by F–F repulsions. At ambient, each F has one hydrogen-bonded F neighbor at 2.26 Å and four K at 2.76 Å. The next nearest neighbors are four F in the same *xy* plane at 3.09 Å and six F above and below the plane at 4×3.76 Å and 2×3.82 Å. The shortest four distances are 18% shorter than the F–F distances in KF (3.77 Å), which presumably accounts for the greater stiffness of the structure in the *xy* plane. The longer distances are similar to those in KF. Note that the hypothetical *Pa*3 structure discussed in the Introduction would have F–F distances (in addition to the short H-bonded one) of 6×3.65 Å and 6×3.88 Å at ambient, all of which are again comparable to the 12×3.77 Å in KF.

The occurrence of short nonbonded F–F distances in the structure can be rationalized as follows. The concave from of the variation of repulsion energy with distance implies that as the next-nearest neighbor environment becomes less regular, repulsion between next-nearest neighbors increases. This is analogous to the distortion theorem of Brown and Shannon (26). The F–F repulsions in KHF_2 are therefore stronger than they would be for a hypothetical version of the structure with all 10 nonbonded F–F distances equal. This condition is uniquely satisfied for $x_F = \frac{1}{6}$, $c/a = 0.943$. For nonbonded F–F = 3.77 Å, the corresponding cell parameters would be $a = 7.15$ Å and $c = 6.74$ Å, the F–H–F distance would be 3.37 Å, and the K–F distance would be 2.92 Å. Clearly, this variant of the structure has excessively long bonding distances relative to that observed. Its cell volume is 58% larger than that observed and 38% larger than that calculated for the *Pa*3 structure. The real structure is evidently derived from it by contraction in the *xy* plane (*c* remains almost constant), so as to attain reasonable H–F and K–F bond lengths. The resulting increase in bond strength more than compensates for the considerable increase in F–F repulsion.

The arrangement of K and F atoms in the *I*4/*mcm* structure is formally identical to that in the large group of intermetallic and interstitial compounds typified by $CuAl_2$ and Fe_2B. In these compounds, repulsion between similarly charged species is unimportant, hence the *c/a* ratio is lower (0.743–0.881). The unconstrained atomic coordinate *x* of the F analog is larger (0.154–0.168 as opposed to 0.143 in KHF_2), which renders the closest 15 interatomic distances much more equal (27–31). In $CuAl_2$, the most distant of these neighbors of the Al is only 25% further away than the nearest, whereas in KHF_2 the longest of these distances is 37% further away than the short F–H–F distance. Furthermore, in the intermetallic phases there is no especially strong bond corresponding to the hydrogen bond in KHF_2, and the equivalent of the K–F distance is actually shorter. Nevertheless, the geometrical similarity to a highly coordinated, ''tetrahedrally close-packed'' intermetallic structure helps to explain the high-pressure stability of tetragonal KHF_2. It is interesting to note that a wide range of difluorides and dioxides without interanionic bonding are either known or predicted to have ''intermetallic'' structures of the cotunnite–Co_2Si–Ni_2In-type (C23, C37, or $B8_b$) at high pressure (32), in which the cation coordination number by anions is 9–11. It is possible that electron density concentrations between anions may stabilize the *I*4/*mcm* structure relative to these in some systems at high pressure. Electron density about half the maximum along Si–O axes has been found between close O–O pairs in the stishovite form of SiO_2 (33), and some models predict that incipient anion–anion bonding will stabilize the pyrite structure relative to the fluorite structure in this compound at higher pressure (34). Since the KHF_2 structure appears to be stable at higher pressures than the pyrite structure, it is possible that silica adopts the *I*4/*mcm* structure under extreme pressure.

ACKNOWLEDGMENTS

This work was initiated under Science and Engineering Council (SERC) Grant GR/G04844 to SMC and Dr. D. M. Adams (University of Leicester). We thank the SERC for providing beam time at the Daresbury SRS and for the support of the Daresbury staff. We also thank Dr. J. Haines for his interest and encouragement in this project.

REFERENCES

1. R. Kruh, K. Fuwa, and T. McEver, *J. Am. Chem. Soc.* **78,** 4256 (1956).
2. R. W. G. Wyckoff, ''Crystal Structures,'' Vol. 2, p. 277. Wiley–Interscience, New York, 1964.
3. J. Bruinink, *in* ''Fast Ion Transport in Solids, Solid-State Batteries and Devices: Proceedings of the NATO Advanced Study Institute, Belgirate, Italy, 1972'' (W. van Gool, Ed.), p. 157. North-Holland, Amsterdam, 1973.
4. L. E. Nagel and M. O'Keefe, *in* ''Fast Ion Transport in Solids, Solid-State Batteries and Devices: Proceedings of the NATO Advanced

Study Institute, Belgirate, Italy, 1972'' (W. van Gool, Ed.), p. 165. North-Holland, Amsterdam, 1973.
5. Y. Furukawa and H. Kirayama, *Bull. Chem. Soc. Jpn.* **51,** 3438 (1978).
6. R. S. Bradley, D. C. Munro, and S. I. Ali, *J. Inorg. Nucl. Chem.* **32,** 2513 (1970).
7. R. W. Fink and E. F. Westrum Jr, *J. Phys. Chem.* **60,** 800 (1956).
8. M. L. Davis and E. F. Westrum Jr. *J. Am. Chem. Soc.* **65,** 338 (1961).
9. J. Haines and A. G. Christy, *Phys. Rev. B* **46,** 8797 (1992).
10. A. G. Christy, R. J. Angel, J. Haines, and S. M. Clark, *J. Phys. Condens. Matter* **6,** 3125 (1994).
11. A. G. Christy, J. Haines, and S. M. Clark, *J. Phys. Condens. Matter* **4,** 8131 (1992).
12. F. Gronvold and E. F. Westrum Jr, *J. Chem. Thermodynam.* **8,** 1039 (1976).
13. H. G. von Schnering and N.-K. Goh, *Naturwissenschaften* **61,** 272 (1974).
14. J. Haines and J. M. Léger, *Phys. Rev. B* **48,** 13344 (1993).
15. S. M. Clark, *Nucl. Inst. Meth. A* **276,** 381 (1989).
16. S. M. Clark, *Rev. Sci. Inst. IIB* **63,** 1010 (1992).
17. W. I. F. David, M. W. Johnson, K. J. Knowles, C. M. Moreton-Smith, G. D. Crosbie, E.P. Campbell, S. P. Grahamand, and J. S. Lyall JS, Rutherford Appleton Laboratory Internal Report RAL-86-102 (1986).
18. A. D. Murray, J. K. Cockroft, and A. N. Fitch, Powder Diffraction Program Library, University College London, 1990.
19. D. L. Decker, *J. Appl. Phys.* **42,** 3239 (1971).
20. H. L. Carrell and J. Donohue, *Israel J. Chem.* **10,** 195 (1972).
21. F. D. Murnaghan, *Proc. Nat. Acad. Sci. USA* **30,** 244 (1944).
22. F. Birch, *J. Geophys. Res.* **57,** 227 (1952).
23. T. Takahashi and W. A. Bassett, *Science* **145,** 483 (1964).
24. A. P. Jephcoat, H.-K. Mao, and P. M. Bell, *J. Geophys. Res.* **91,** 4677 (1986).
25. A. G. Christy, *Acta Crystallogr. Sect. B* **51,** 753 (1995).
26. I. D. Brown and R. D. Shannon, *Acta Crystallogr. Sect. A* **29,** 266 (1973).
27. E. E. Havinga, H. Domsma, and P. Hokkeling, *J. Less-Common Met.* **27,** 169 (1972).
28. E. E. Havinga, *J. Less-Common Met.* **27,** 187 (1972).
29. E. E. Havinga and H. Domsma, *J. Less-Common Met.* **27,** 269 (1972).
30. E. E. Havinga, H. Domsma, and J. M. Kanis, *J. Less-Common Met.* **27,** 281 (1972).
31. W. B. Pearson ''The Crystal Chemistry and Physics of Metals and Alloys,'' p. 607. Wiley–Interscience, New York, 1972.
32. J. M. Léger, J. Haines, A. Atouf, O. Schultz, and S. Hull, *Phys. Rev. B* **52,** 13247 (1995).
33. R. J. Hill, M. D. Newton, and G. V. Gibbs, *J. Solid State Chem.* **47,** 185 (1983).
34. K. T. Park, K. Terakura, and Y. Matsui, *Nature* **336,** 670 (1988).